Experimental Validation Through a Parallel Computation Algorithm for Evaluation Uncertainty of the Mathematical Model of Direct Expansion Solar Assisted Heat Pump

Willian M. Duarte[1,*], Tiago F. Paulino[2], Wendel M. Duarte[3], Antônio A.T. Maia[1], and Luiz Machado[1]

[1]*Post-Graduate Program in Mechanical Engineering, Federal University of Minas Gerais (UFMG), Belo Horizonte-MG, Brazil*

[2]*Post-Graduate Program in Mechanical Engineering, Federal Center of Technological Education of Minas Gerais (CEFET-MG), Belo Horizonte (MG), Brazil*

[3]*Federal Center of Technological Education of Minas Gerais (CEFET-MG), Post-Graduate Program in administration, Belo Horizonte (MG)*

Abstract: This paper presents the development of a mathematical model for a direct-expansion solar-assisted heat pump (DX-SAHP) operating in steady-state. The mathematical model was implemented using the scientific software EES and using a code written in Python. It was utilized a lumped parameter model for the heat exchangers and a semi-empirical model for the compressor. The mathematical model was validated using experimental data of a DX-SAHP running with R134a. Two hundred simulations were made combining different correlations for estimating the convective heat transfer coefficient in the evaporator/collector. The Mean Absolute Deviation (MAD) and the Mean Deviation (MD) between the theoretical and experimental values for the COP were 2.6±1.8 % and 0.9±1.8 %, respectively. The MAD and MD between the discharge temperature were 1.56±0.16 % and -1.45±0.16 %. The mean difference between the results using EES and Python were 1.4 %. The use of Python with parallel computing for uncertainty analyses, reduced the simulation time in 88 % if compared with EES. The model in Python is available as open-source through the platform Google Colaboratory.

Keywords: Model, DX-SAHP, Uncertainty, Parallel Computing, Open-source.

1. INTRODUCTION

Replacing electric heaters by heat pumps has several advantages such as reducing operating costs, reducing energy consumption, and reducing greenhouse gas emissions. According to recent studies, employing renewable energies like solar energy [1-3], geothermal energy [4-6], wind power [7] and bio-gas [8] is one way to increment the COP of the heat pumps. Different Solar-Assited Heat Pump (SAHP) setups that were found in the literature review presented by Buker and Riffat [9]. According to the authors, a Direct-Expansion Solar-Assisted Heat Pump (DX-SAHP) is a device where the refrigerant passes via the solar collector/evaporator. In the Indirect Expansion Solar-Assisted Heat Pump (IX-SAHP) the evaporator and solar collector are different components and brine flows through the solar collector.

Various studies using mathematical models for DX-SAHP were found in the literature. Most of them are complete models of the system, but some studies modeled partially the heat pump [10-13]. The studies using complete models of DX-SAHP are summarized in Table **1**. In column collector type UFP represents uncovered flat plate, CFP represents covered flat plate and PVT represents photo-voltaic thermal hybrid solar collectors. The information missing in some studies is marked with '-', and information not applicable is marked with N.A.

In the literature consulted most models were validated with experimental data, comparing the COP or the water temperature in the tank or at the outlet of the condenser. Only in the work presented by Chyng *et al*. [14] the authors compared the theoretical and experimental compressor outlet temperature. Predict the discharge temperature of the compressor is important to increase the life span of the compressor. High temperatures in the suction also increase the discharge temperature, resulting in the loss of viscosity of the lubricating. This condition of operation can reduce considerably the life span of the compressor. The performance indicator most used to assess the accuracy of the model was the relative error or mean relative deviation. The relative error for some models is listed in Table **1**. In the early studies presented by Torres-Reyes and Gortari [15], Hawlader *et al*. [16], Ito *et al*. [17], Chaturvedi *et al*. [18] and Chaturvedi and Shen [19] the comparison of the measured and calculated values was made qualitatively plotting both results in the same graphic with the same scale. Additionally, in the studies listed in Tab. 1 it was not evaluated different correlations for the convective

Address correspondence to this article at thePost-Graduate Program in Mechanical Engineering, Federal University of Minas Gerais (UFMG), Belo Horizonte-MG, Brazil;
E-mail: willianmoreiraduarte@gmail.com

E-ISSN: 2410-2199/23

coeficient to assess its influence on the results. Lastly, no computer code is provided for the scientific community.

In the works listed in Table **1**, none of them evaluated the precision of the model through the uncertainty analysis as recommended by ASME [20] during the validation process, although there are in the studies listed in the Table **1** with uncertainty analysis of the experimental results. In fact the there are few studies that relate uncertainty to the model results but none of then uses the method standardized in the Guide to the expression of Uncertainty in Measurement (GUM) presented by BIPM *et al*. [21]. Zhang *et al*. [22] and Zhang *et al*. [23] investigate the impact of model uncertainty on the energy consumption of water source heat pump comparing different models. Frutiger *et al*. [24] presented a refrigerant selection for Heat pump using the Monte Carlo method. Coppitters *et al*. [25] proposed a method for robust design optimization of a Photovoltaic-battery-heat pump system considering uncertainty of some parameter such as electricity price using the the Polynomial Chaos Expansion for uncertainty quantification. A similar study to Coppitters

Table 1: Complete Models of DX-SAHP

Authors	Collector Type	Collector size (m^2)	Refrigerant	Experimental Validation	Relative error (%)	Location	Tank size (L)	Water Temp. (^oC)
Chaturvedi and Shen [19]	UFP	3.4	R12	Yes	-	Norfolk	-	-
Chaturvedi *et al*. [18]	UFP	3.5	R12	Yes	-	Norfolk	-	-
Ito *et al*. [17]	UFP	3.2	R22	Yes	-	Japan	-	30-60
Torres-Reyes and Gortari [15]	UFP	4.5	R22	Yes	-	Guanajuato	-	-
Hawlader *et al*. [16]	UFP	3.0	R134a	Yes	-	Singapore	250	55
Chyng *et al*. [14]	UFP	1.9	R134a	Yes	10 (max)	Taiwan	-	52-56
Kuang *et al*. [40]	UFP	2.0	R22	Yes	5-30	Shanghai	150	50
Chata *et al*. [41]	UFP	-	R404A, R407C, R410A, R12, R22 and R134a	No	N.A.	-	-	-
Xu *et al*. [42]	PVT	2.3	R22	No	N.A.	Nanjing	150	50
Chow *et al*. [43]	UFP	12	R134a	No	N.A.	Hong Kong	1500	50
Kong *et al*. [44]	UFP	4.2	R22	Yes	1-4.6	Shanghai	150	50
Moreno-Rodríguez *et al*. [45]	UFP	5.6	R134a	Yes	10 (max.)	Madri	300	51
Chaturvedi *et al*. [46]}	UFP	1-5	R134a	No	N.A.	Norfolk	-	50-70
Sun *et al*. [47]	UFP	2.0	-	No	N.A.	Shanghai	150	55
Deng and Yu [48]	CFP	2.5	R134a	No	N.A.	-	150	55
Kong *et al*. [49]	UFP	4.2	R410A	No	N.A.	-	150	50
Mohamed *et al*. [50]	UFP	4.2	R407C	Yes	4 (max.)	Nottingham	200	50
Duarte [51]	UFP	1.6	R134a, R600a, R290, R1234yf and R744	Yes	≈5(max.) 1.6(mean)	Belo Horizonte	200	65
Rabelo *et al*. [52]	UFP	1.3-6	R134a and R290	Yes	-	Belo Horizonte	200	65
Kong *et al*. [53]	UFP	2.1	R134a	Yes	10 (max.)	-	200	60
Diniz *et al*. [54]	UFP	1.6	R744	Yes	-	Belo Horizonte	200	≈40
Wang *et al*. [55]	UFP	2.1	R134a	Yes	-	-	200	30-50
Ma *et al*. [56]}	UFP	≈2.3	R22	Yes	13 (max.)	-	-	-
Dai *et al*. [57]	UFP	100	R134a	No	N.A.	Beijing	-	-
Humia [58]	UFP	1.6	R744	Yes	5-7.5	Belo Horizonte	200	60

et al. [25] was presented by Moarry [26] but for a Ground Source Heat Pumps (GSHP) and by Nielsen *et al*. [27] for an Air Source Heat Pumps (ASHP). Lastly, an experimental validation, without considering the uncertainty of the model, was made by some scholar for Indirect-Expansion Solar-Assisted Heat Pump (IX-SAHP) [28, 29], for GSHP [30-32], for Solar-Assisted Ground Source Heat Pump (SAGSHP) [33] and for refrigeration system [34-36]. One of the possible reasons for the aforementioned authors not to perform model uncertainty analysis is the fact that the computational time for calculating model uncertainty is very high. One possible strategy to reduce the computational time is the use of parallel processing as done by some authors [37-39].

Three research gaps in conjunction with the previous studies of described above was identified: (i) No study present a open source model; (ii) No study is involved in the results uncertainty of the model during the experimental validation; (iii) The flow conditions in the solar evaporation can be very different from the conditions used in the development of the correlation, but no study tested different correlations and investigated the influence on the results and uncertainty. This work presents a mathematical model for a DX-SAHP to fill the above-mentioned gaps. Two hundred simulations were performed combining different correlations for estimating the convective heat transfer coefficient. The best combination was employed in the validation tests using experimental data of COP and discharge temperature, taking into account the uncertainty of theoretical and experimental results. To the best of the authors' knowledge, this is the first work that considers uncertainty during the comparison between theoretical and experimental results using parallel computing.

2. MATHEMATICAL MODEL

The refrigerant fluid chosen for this work was the R134a because it is more suitable for DX-SAHP than R410A, R407C and R404A, as indicated by Chata *et al*. [41]. Also, R134a is one of the refrigerants most used in the recent studies of DX-SAHP [59-62, 52] and lastly, the refrigerant utilized in the actual testing was what allowed the mathematical model to be validated.

Equation Engineering Solver (EES) and Python 3.8 were used to create a quasi-steady-state model to assess the performance of DX-SAHP in producing DHW (Domestic Hot Water). The pipeline was deemed to be two meters long for the purposes of the refrigerant inventory charge, and the losses in the tubes between components were thought to be insignificant. A lumped model was applied, with the evaporator/solar collector and condenser being considered to be isobaric. The modeling equation for each component is provided below.

2.1. Compressor Model

As mentioned by de Paula *et al*. [63], in the literature, there are detailed models of compressors but these models required many parameters and geometrical details that are not provide by the manufactures of hermetic compressors [64, 65, 66]. Additionally, the compressor model used in the complete model of the refrigeration system is a simple one as those employed in other studies [49, 67, 68]. The mass flow rate ($\dot{m}$) for a reciprocating compressor with constant rotation speed is given by [61]:

$$\dot{m} = \rho_1 n V_s \eta_{vol} \tag{1}$$

where n is the rotation speed (3500 rpm), V_s is the compressor swept volume (7.95 cm3/rev.), η_{vol} is the volumetric efficiency, and the subscript 1 denotes the compressor intake or evaporator outlet. The thermodynamic properties were calculated using the internal library of EES [69] or the library CoolProp [70] in the Python version. The compressor electric power ($\dot{W}$), was calculated using the isentropic compression process as reference as made by Minetto [71]:

$$\dot{W} = \frac{\dot{m}(i_{2S} - i_1)}{\eta_g} \tag{2}$$

where i is the refrigerant specific enthalpy and η_g is the global efficiency, and the subscript $2S$ denotes the compressor outlet when taking into account an isentropic process. The global and volumetric efficiency were determinate fitting polynomial equation using the pressure ratio as the independent variable to the compressor performance map provided by the manufacturer as performed by [71]. To obtain with good precision, the discharge temperature of the compressor (T_2) an isentropic efficiency (η_i) was considered, and the enthalpy at the exit of the compressor evaluated as follow:

$$i_2 = \frac{i_{2S} - i_1}{\eta_i} + i_1 \tag{3}$$

2.2. Evaporator Model

As mentioned by Duarte *et al*. [72], there are many studies use distributed heat exchangers models [73-75], but such models require much computational effort if compared with lumped models. Additionally, some studies demonstrate that the concentrated model can be used to quickly assess system performance [76-78]. As made by some scholar [52, 53, 55] the pressure of

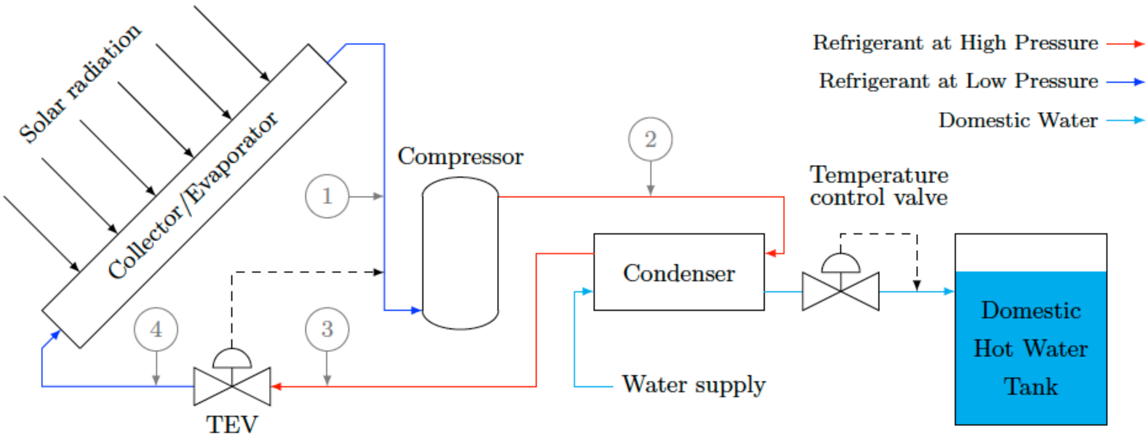

Figure 1: Schematic diagram of DX-SAHP used for a validation model.

the refrigerant was assumed constant in the condenser and in solar collector/evaporator. The refrigerant in the evaporator receives heat at the following rate:

$$\dot{Q}_{re} = \dot{m}(i_1 - i_4) \tag{4}$$

where the thermostatic valve outlet or evaporator intake is indicated by the subscript 4. In order to assess the energy gain in a flat plate collector ($\dot{Q}_{col}$) under steady-state conditions the following equation is suggested by [44]:

$$\dot{Q}_{col} = A_e F'[S - U_{ev}(\overline{T}_r - T_a)] \tag{5}$$

where T_a is the ambient air temperature, $\overline{T}_r$ is the average temperature of the refrigerant fluid, U_{ev} is overall heat loss coefficient, A_e is the area of the evaporator (1.65 m^2) and S is the net radiation absolved. The collector effectiveness factor (F') is derived using the Hottel-Whilliar-Bliss model provided by Duffie and Beckman (2013), taking into account the resistance to heat flow owing to the bond between the collection plate and tube, as follows:

$$F' = \frac{1}{U_{ev}}\left\{W\left[\frac{1}{U_{ev}[D_o + F(W-D_o)]} + \frac{1}{\pi D_i h_i}\right]\right\}^{-1} \tag{6}$$

where W is the distance between the tubes in the evaporator, F is the fin efficiency, D_o is the outer diameter, D_i is the inner diameter, and h_i is the internal convective coefficient. The fin efficiency may be calculated as follows:

$$F = \frac{\tanh[(W-D_o)/2\sqrt{U_{ev}/(k\delta)}]}{(W-D_o)/2\sqrt{U_{ev}/(k\delta)}} \tag{7}$$

where δ is the thickness of the fin (1mm) and k is the thermal conductivity. The net radiation absolved is calculated in follows [49]:

$$S = aI - \varepsilon\sigma\left(\overline{T}_r^4 - T_{sky}^4\right) \tag{8}$$

where a is the absorptivity, I is the solar radiation intensity normal to the evaporator, ε is the emissivity, σ is the Stefane-Boltzmann constant, and T_{sky} is the sky temperature. The sky temperature was calculated using the approach described by Gliah *et al.* [79] (Eq. 9) using the Angstrom correlation proposed by Berdahl and Fromberg [80] for sky emissivity (Eq. 10).

$$T_{sky} = \left(\varepsilon_{sky} T_a^4\right)^{1/4} \tag{9}$$

$$\varepsilon_{sky} = 0.734 + 0.0061\left(T_{dp} - 273.15\right) \tag{10}$$

Kong *et al.* [44] presented a collector total heat loss coefficient that is calculated by:

$$U_{ev} = h_o + 4\varepsilon\sigma T_a^3 \tag{11}$$

where the external convective coefficient (h_o) is obtained by the correlations for free or forced convection. For natural flow on horizontal flat plate, some authors [81, 82, 83] pointed the correlation of Lloyd and Moran [84], tested for $10^5 < Ra < 10^{10}$ and shown on EQ. 12. For this flow configuration, the characteristic length is defined as the ratio between area and plat perimeter. To determine the Nusselt number the Churchill and Chu [85] correlation is used EQ. 13 for $0.1 < Ra < 10^9$ and EQ. 14 for $10^9 < Ra < 10^{12}$.

$$Nu = 0.27Ra^{1/4} \tag{12}$$

$$Nu = 0.68 + \frac{0.67Ra^{1/4}}{\left(1+(0.492/Pr)^{9/16}\right)^{4/9}} \tag{13}$$

$$Nu = \left[0.825 + \frac{0.387Ra^{1/6}}{\left(1+(0.492/Pr)^{9/16}\right)^{8/27}}\right]^2 \tag{14}$$

$$Ra = \frac{g\beta\rho^2|\Delta T|L_{ch}^3}{\mu^2}Pr \tag{15}$$

In these equations β is the coefficient of thermal expansion, ΔT is the temperature difference between the surface and the quiescent fluid, and L_{ch} is the characteristic length. All proprieties are evaluated at film temperature, except β which is evaluated at quiescent fluid temperature. For inclined plates, top-cold and bottom-hot, Bergman *et al*. [81] propose to evaluate the convective coefficient for vertical plate, replacing the value of the gravity by the expression $g \cdot \sin(\theta)$ in the Rayleigh number. Subsequently, must repeat the process using the expression $g \cdot \cos(\theta)$ in the correlations for horizontal plate and adopting the highest value.

To calculated the Nusselt number in forced flow Neils and Klein [82] suggest the correlation of Churchill and Ozoe [86], EQ. 16, for laminar flow, $Re < Re_{crit} = 5 \cdot 10^5$, and the EQ. 17 for turbulent flow. In equation 17 Nu_{Crit} is evaluated using EQ. 16 for $Re = Re_{crit}$. Neils and Klein [82] recommend the use of forced flow if Péclet number (EQ. 18) is greater than 100.

$$Nu = \frac{0.6774Re^{1/2}Pr^{1/3}}{\left[1+(0.0468/Pr)^{2/3}\right]^{1/4}} \quad (16)$$

$$Nu = Nu_{crit} + 0.037Pr^{1/3}(Re^{0.8} - Re_{crit}^{0.8}) \quad (17)$$

$$Pe = RePr \quad (18)$$

The internal convective coefficient (h_i), in the boiling region, is given by Shah [87] and it is the largest value given by the EQ. 19 to 22. B_A is equal to Co if horizontal with $Fr_L \geq 0.04$ or vertical and equal to $0.38CoFr_L^{-0.3}$ f horizontal with $Fr_L < 0.04$. $B_B = 14.7$ for $Bo \geq 0.0011$ and $B_B = 15.4$ for $Bo < 0.0011$. $B_C = 2.1 - 0.008We_V - 110Bo$ if $B_C \geq 1$ and $B_C = 1$ if $B_C < 1$ or $Fr_L < 0.01$.

$$h = 1.8B_A^{-0.8}B_Ch_L \quad (19)$$

$$h = 230Bo^{0.5}B_Ch_L \quad (20)$$

$$h = B_BBo^{0.5}exp(2.74B_A^{-0.1})B_Ch_L \quad (21)$$

$$h = B_BBo^{0.5}exp(2.74B_A^{-0.15})B_Ch_L \quad (22)$$

In these equations, h_L is the liquid heat transfer coefficient calculated by Dittus and Boelter [88] (EQ. 23), the Froud number is calculated by EQ. 24, the convection number by EQ. 25, the Weber number by EQ. 27, and the boiling number by EQ. 28.

$$Nu = 0.023Re^{0.8}Pr^{0.4} \quad (23)$$

$$Fr_L = \frac{G^2}{\rho_L^2 g D_i} \quad (24)$$

$$Co = \left(\frac{1-x}{x}\right)^{0.8}\left(\frac{\rho_V}{\rho_L}\right)^{0.5} \quad (25)$$

$$G = \frac{\dot{m}}{A} \quad (26)$$

$$We_V = \frac{G^2D_i}{\rho_V\sigma'} \quad (27)$$

$$Bo = \frac{q}{G(i_V - i_L)} \quad (28)$$

In fact, the flow in the heat pump evaporator it is relatively peculiar. The flow alternates between ascending and descending and it is inclined in relation to the horizontal. Such conditions are not normally implemented on test benches where correlations for heat transfer are tested. Therefore, it is interesting to test different equations to evaluate the heat transfer in the heat pump evaporator. Alternatively, to the correlation of Shah [87] it was tested the correlation of Liu and Winterton [89] and Sun and Mishima [90]. The correlation of Liu and Winterton [89] is given by Eq. 29 to 33, where h_{po} is evaluated using the correlation of Cooper [91] (Eq. 33) and h_L is evaluated using the correlation of Dittus and Boelter [88] (EQ. 23).

$$h = \sqrt{(B_A \cdot h_L)^2 + \left(B_C \cdot h_{po}\right)^2} \quad (29)$$

$$B_C = (1 + 0.055B_A^{0.1}Re_{lo}^{0.16})^{-1} \quad (30)$$

$$B_A = [1 + xPr_l(\rho_L/\rho_V - 1)]^{0.35} \quad (31)$$

$$Re_{lo} = \frac{GD_i}{\mu_L} \quad (32)$$

$$h_{po} = 55\left(\frac{P}{P_{crit}}\right)^{0.12} q^{2/3}\left[-\log_{10}\left(\frac{P}{P_{crit}}\right)\right]^{-0.55} M^{-0.5} \quad (33)$$

The correlation of Sun and Mishima [90] is given by Eq. 34 and We_L is evaluated as Eq. 27 but using the liquid density.

$$Nu = \frac{6Re_{lo}^{1.05}Bo^{0.54}}{We_L^{0.191}(\rho_L/\rho_V)^{0.142}} \quad (34)$$

The internal convective coeﬃcient (h_i), in the super-heated vapor region, is calculated by Gnielinski [92] that is the most recommended correlation for turbulent fully developed single phase flow [93, 81, 82]. The correlation of Gnielinski [92] in described in EQ. 35 and Neils and Klein [82] suggest the correlation proposed by Zigrang and Sylvester [94] for Darcy friction factor (f) describe in EQ. 36.

$$Nu = \frac{(f/8)(Re-1000)Pr}{1+12.7(f/8)^{1/2}(Pr^{2/3}-1)} \quad (35)$$

$$f = -4\log_{10}\left[\frac{\epsilon}{3.7D} - \frac{5.02}{Re}\log_{10}\left(\frac{\epsilon}{3.7D} + \frac{13}{Re}\right)\right]^{-2} \quad (36)$$

2.3. Coaxial Condenser Model

The balance of energy in the refrigerant at the condenser is evaluated as follow:

$$\dot{Q}_{cond} = \dot{m}_r(i_2 - i_3) \quad (37)$$

Assuming no heat loss in the coaxial condenser, the balance of energy in the water is given by:

$$\dot{Q}_{cond} = \dot{m_w} C_w (T_{wo} - T_{wi}) \quad (38)$$

The effectiveness-NTU technique is used to determine the heat transfer rate in the condenser. The effectiveness (ξ or ξ') of a concentric heat exchanger is evaluated as follows [81]:

$$\xi = \frac{Q_{cond}}{\dot{C}_{mim}(T_2 - T_{wi})} \quad (39)$$

$$\xi' = \frac{1-\exp[-NTU(1-\dot{C}_{min}/\dot{C}_{max})]}{1-\exp[-\text{NTU}(1-\dot{C}_{min}/\dot{C}_{max})]\dot{C}_{min}/\dot{C}_{max}} \quad (40)$$

where $\dot{C}_{min}$ and $\dot{C}_{max}$ is the equal to $\dot{C_r}$ or $\dot{C_w}$, whichever is smaller and bigger, respectively. The refrigerant and water heat capacity rate are given by:

$$\dot{C_w} = \dot{m}_w \, C_w \quad (41)$$

$$\dot{C_r} = \dot{m_r} \overline{C}_r \quad (42)$$

In these equations, the mean specific heat of the refrigerant ($\overline{C}_r$) (is evaluated by EQ. 43 [51] and the Number of Transfer Units (NTU) by EQ. 44 [81].

$$\overline{C}_r = \frac{i_2 - i_3}{T_2 - T_3} \quad (43)$$

$$NTU = \frac{UA}{\dot{m_w} C_w} \quad (44)$$

The UA value is calculated as follows [83]:

$$UA = \left(\frac{1}{\overline{h}_r \pi D_{ii} L_{cond}} + \frac{ln(D_{ii}/D_{io})}{2\pi k L_{cond}} + \frac{1}{\overline{h}_w \pi D_{oi} L_{cond}}\right)^{-1} \quad (45)$$

where the D_{ii} is the inner diameter of inner tube (4.76mm), D_{oi} is the outer diameter of inner tube (6.35mm), L_{cond} is condenser length (5.5m), the mean water HTC ($\overline{h}_w$). The mean refrigerant HTC ($\overline{h}_r$) is calculated assuming that the enthalpy varies linearly with length and using the correlation of Gnielinski [92] for h_r if $i \geq i_V$ or $i \leq i_L$ and the correlation of Shah [95] if $i_L < i < i_V$. Shah [95] proposed the following equations for the flows regimes I, II and III:

$$h_I = h_L \left(1 + \frac{3.8}{B^{0.95}}\right)\left(\frac{\mu_L}{14\mu_V}\right)^{0.0058+0.557p} \quad (46)$$

$$h_{II} = h_I + h_{III} \quad (47)$$

$$h_{III} = 1.32 Re_L^{-1/3} \left[\frac{\rho_L(\rho_L - \rho_V) g k_L^3}{\mu_L^2}\right]^{(1/3)} \quad (48)$$

$$B = p^{0.4}\left(\frac{1}{x-1}\right)^{0.8} \quad (49)$$

where h_L is the liquid heat transfer coefficient calculated by EQ. 23 and Re_L is calculated by EQ. 50. The ranges that occur the regime I and III are presented in Table **2**. If the Regime is neither I nor III by the criteria below, it is considered Regime II. The Weber number (We) and dimensionless vapor velocity (v) are calculated by EQ. 27 and 51, respectively

$$Re_L = \frac{G(1-x)D_i}{\mu_L} \quad (50)$$

$$v = \frac{xG}{[gD\rho_V(\rho_L - \rho_V)]^{0.5}} \quad (51)$$

The Nusselt numbers for laminar flow in annular regions are presented in Table **3** regarding the ratio between the inner tube outside diameter (D_{io}) and the outer tube inner diameter (D_{oi}) [81, 93]. To evaluate the Nusselt number in ranges between the rows of Table **3** the EQ. 52 and 53 was fitted to the data with coefficient of determination (R²) of 96.8% and 97.5%, respectively. In fact, in the condenser the flow conditions were neither uniform temperature nor uniform heat flux, but the simulations showed better results using the uniform temperature equation. For the turbulent flow in annular regions, Neils and Klein [82] recommend the use of EQ. 35 and 36 using the hydraulic diameter instead of the diameter.

Table 3: Nusselt Number for Fully Developed Laminar Flow in Annular Regions

D_{io}/D_{oi}	Uniform Temperature	Uniform Heat Flux
0.02	32.337	32.705
0.05	17.460	17.811
0.10	11.560	11.906
0.25	7.3708	7.7535
0.50	5.7382	6.1810
1.00	4.8608	5.3846

$$Nu = 4.6005\left(\frac{D_{io}}{D_{oi}}\right)^{-0.464} \quad (52)$$

Table 2: Flows Regime of the Correlation of Shah [95]

	Horizontal Flow	Vertical Flow
Regime I	$We_V > 100$ and $v \geq 0.98(B + 0.263)^{-0.62}$	$We_V > 100$ and $v \geq (0.73 + 2.4B)^{-1}$
Regime III	$We_V > 20$ and $v \leq 0.95(1.254 + 2.27B^{1.249})^{-1}$	$We_V > 20$ and $v \leq 0.89 - 0.93\exp(-0.087B^{-1.17})$

$$Nu = 4.1981 \left(\frac{D_{io}}{D_{oi}}\right)^{-0.487} \quad (53)$$

Kong *et al*. [44] recommend a heat leakage coefficient (ζ) of 95% to account for heat loss at the water tank and in the connecting tubes before and after the condenser.

$$\zeta = \frac{Q_t}{Q_{cond}} \quad (54)$$

2.4. Performance Indicators

Many authors [44, 49, 40] defined the coefficient of performance (COP) as follow:

$$COP = \frac{\zeta \cdot \dot{Q}_{cond}}{\dot{W}} \quad (55)$$

To compare the accuracy of the model, the most used metrics are the Mean Absolute Deviation (MAD) and Mean Deviation (MD). For the COP, the MAD and MD are evaluated as showed in EQ. 56 and 57. The compressor outlet temperature (T_2) is calculated in a similar way.

$$MAD = \frac{1}{n}\sum_{j=1}^{n}\left|\frac{COP_{calc}-COP_{exp}}{COP_{exp}}\right| \quad (56)$$

$$MD = \frac{1}{n}\sum_{j=1}^{n}\left(\frac{COP_{calc}-COP_{exp}}{COP_{exp}}\right) \quad (57)$$

2.5. Numerical Procedure

The pressure of the refrigerant is not known and cannot be obtained from the equations presented so far. An algorithm to calculate this pressure was presented by Kong *et al*. [44], but in this study, the author used a DX-SAHP with an immersed condenser, and the mass of refrigerant was an input of the mathematical model. A simplified algorithm explaining how these pressures were obtained is shown in Figure **2** for a heat pump with a coaxial condenser. The secant method mentioned in Figure **2** is described in detail by Chapra *et al*. [96]. The errors E_e and E_c, in percent, is given by:

$$E_e = \left|\frac{\dot{Q}_{re}-\dot{Q}_{col}}{\dot{Q}_{re}}\right| \cdot 100 \quad (58)$$

$$E_c = \left|\frac{\xi-\xi'}{\xi}\right| \cdot 100 \quad (59)$$

The final values for evaporating pressures were assumed as the initial guess for the next iteration to reduce the computational time. Bounds were set for the evaporating and condensing absolute pressures since the secant method can lead to negatives values. These details were described in the main program available in the Google Colaboratory through the link at the end of the paper. The Python code also includes compressor data for additional ecological refrigerants used in the study provided by Duarte [51], as well as the refrigerant charge calculation utilized in the model presented by Duarte [51]. Some of the correlations mentioned above were not programmed by the author but imported from the Python libraries published by Bell and Rutman [97] and Bell *et al*. [98].

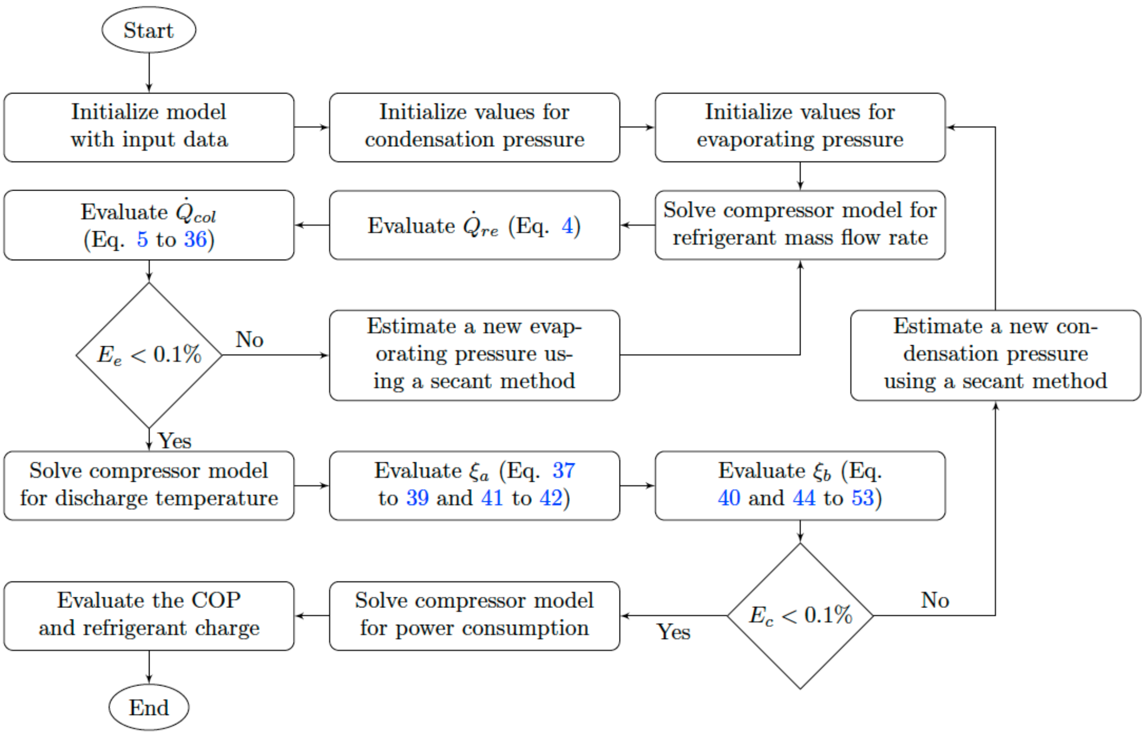

Figure 2: Model calculation algorithm.

2.6. Uncertainty Analysis and Parallel Computing

To evaluate the uncertainty of mathematical model the most two methods used are the GUM method [21] and the Monte Carlo method [99]. Some authors shown that the uncertainty obtained by both method are similar [100, 101] and BIPM *et al.* [99] do not recommend the Monte Carlo method for complex models as that one presented in this article due the large computational time. The output variables of the DX-SAHP model were calculated considering the uncertainties from the input variables. The measurements involved in this work were considered random and uncorrelated, and evaluated according to BIPM *et al.* [21]. For example, the combined uncertainty of the sky temperature (T_{sky}), represented by t_{sky} and can be obtained using the Eq. 9 and 10 and the following equation:

$$t_{sky} = \sqrt{\left[\frac{\partial T_{sky}}{\partial T_a} t_a\right]^2 + \left[\frac{\partial T_{sky}}{\partial T_{dp}} t_{dp}\right]^2} \quad (60)$$

Any other output variables were obtained using equations similarly to Eq. 60. Evidently, the partial derivatives can be obtained algebraically for the combined uncertainty of T_{sky}, but for other output variables it may not be possible. In these cases, BIPM *et al.* [21] suggest a procedure using numerical methods:

$$t_{sky} = \sqrt{\left[\frac{T_{sky}\langle T_a + t_a, T_{dp}\rangle - T_{sky}\langle T_a - t_a, T_{dp}\rangle}{2}\right]^2 + \left[\frac{T_{sky}\langle T_a, T_{dp} + t_{dp}\rangle - T_{sky}\langle T_a, T_{dp} - t_{dp}\rangle}{2}\right]^2} \quad (61)$$

where $T_{sky}\langle T_a, T_{dp}\rangle$ represents the numerical function used to calculate T_{sky} using as input variable T_a and T_{dp}.

Despite the fact that the heat pump has components that work in parallel (evaporator, condenser, compressor, expansion device, etc) for the mathematical model the properties at the outlet of a component are necessary for the next component, in such a way, that there are no models in the consulted literature that use parallel processing to calculation of the model of a heat pump. In fact, to calculate the sky temperature with its respective uncertainty it is necessary to run the function that calculates the sky temperature five times, once to calculate the base result and four times to calculate uncertainty. Therefore, it is an opportunity to use parallel processing to speed up calculations involving a mathematical model. Figure **3** shows the algorithm used for parallel computation of uncertainty of T_{sky}.

Before running all the simulations with all the correlations and all the experimental data, a set of simulations was made for a specific condition in order to determine which are the input variables whose uncertainties most significantly impact the output variables of the model. For example, the acceleration of gravity that was used in the model was $9.7838163 \pm 0.0000004 m/s^2$ measured at the university and presented by Soares [102]. The impacts of the uncertainty of the acceleration of gravity on the model output variables are negligible compared to their impacts of the uncertainties of the ambient temperature. Therefore, nine variables that significantly impact the model's output variables were used in the model's uncertainty analysis: ambient temperature, solar radiation, wind speed, atmospheric pressure water temperature at the condenser inlet, water temperature at the condenser outlet, sky temperature, subcooling, and superheating. In the analysis of the uncertainty of the model, 19 parallel processes were used, 18 to calculate the uncertainty in one for the base result. In the next section, the time needed to carry out simulations with different software and different processing strategies will be compared, so the simulations were made in the computer whose specifications are shown in Table **4**.

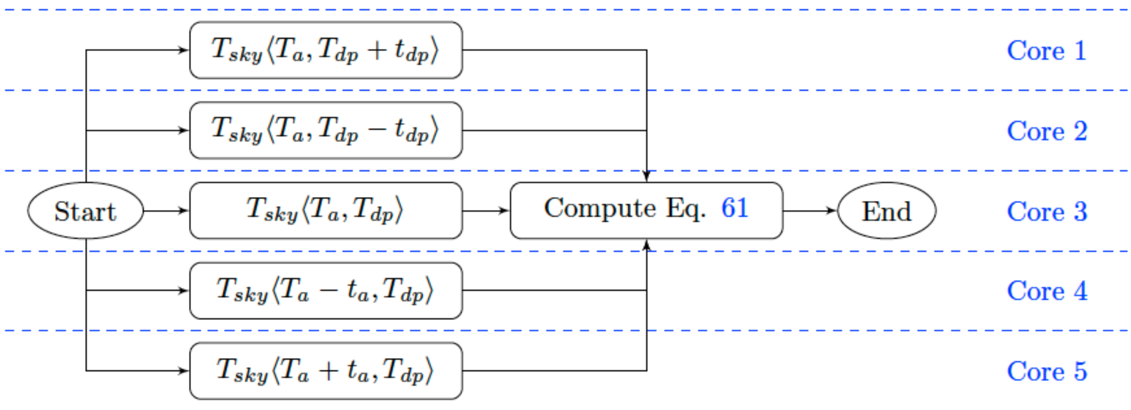

Figure 3: Algorithm for parallel computation of uncertainty.

Table 4: Computer Specification Used In the Simulations

	Manufacturer	Specification or Version
Server	Dell	PowerEdge T440
Processor	Intel	Xenon(R) Silver 4108, 1.8Ghz, 16 core
RAM memory	-	16GB DDR4
Operating system	Windows server	2016

3. RESULTS

3.1. Compressor Efficiency

The 18 data points of volumetric and global efficiency, calculated using the performance map provided by the compressor manufacturer, are shown in Figure **4** with their respective uncertainty (5%). The equation 62 and 63 were fitted to the data using standard tools and plotted in Figure **4.** In these equations, P is the refrigerant pressure. The fitted curves pass through the uncertainty range of all data points.

$$\eta_v = -0.0143\left(\frac{P_2}{P_1}\right) + 0.915 \tag{62}$$

$$\eta_g = -0.0004\left(\frac{P_2}{P_1}\right)^2 + 0.0104\left(\frac{P_2}{P_1}\right) + 0.4839 \tag{63}$$

The coefficient of determination (R^2) for volumetric efficiency is 97.6 % and for global efficiency is 94.4 %. Additionally, the fitted curves pass through the uncertainty range of all data points. The MAD and MD of volumetric efficiency are respectively 0.05 % and 1.5 % and the MAD and MD of global efficiency are respectively -0.41% and 1.4%.

3.2. DX-SAHP Model Validation

The model validation was performed comparing the experimental results using a R134a DX-SAHP, presented in [103] and [51]. Experimental results are shown in the Table **5**. During the experimental tests the subcooling was in the range of 6.5$\pm$1.4°C. In Table **5**, the uncertainty in the water inlet temperature (T_{wi}), water outlet temperature T_{wo}, ambient temperature (T_a) and compressor discharge temperature (T_2) was $\pm$1°C, for dew point temperature (T_{dp}) was $\pm$2°C, for the superheating at exit of evaporator (ΔT_{sh}) was$\pm$1.4°C, for the atmospheric pressure was $\pm$2kPa, for the solar radiation (I) was $\pm$5% and for wind speed (u) was $\pm$3%. Because tests one through five were conducted within the laboratory, the sky temperature was considered to be equal to the ambient temperature. The experiments six to ten were performed outside, therefore the sky temperature was calculated using the EQ. 9 and 10 and the combined uncertainty by EQ. 60. The experimental results used to validate the model present good accuracy, and an average of 5.2% of combined uncertainty for COP and 0.3% of uncertainty for discharge temperature.

Theoretical results are shown in the Table **6** and the comparison of theoretical and experimental results is shown in the Figure **5** The MD and MAD of COP of the simulation made in EES are respectively -2.0±1.7% and 3.2±1.7%. The MD and MAD of COP of the simulation made in Python are respectively 1.2±1.8% and 2.6±1.8%. Considering the uncertainty range, there is no meaningful difference of experimental COP

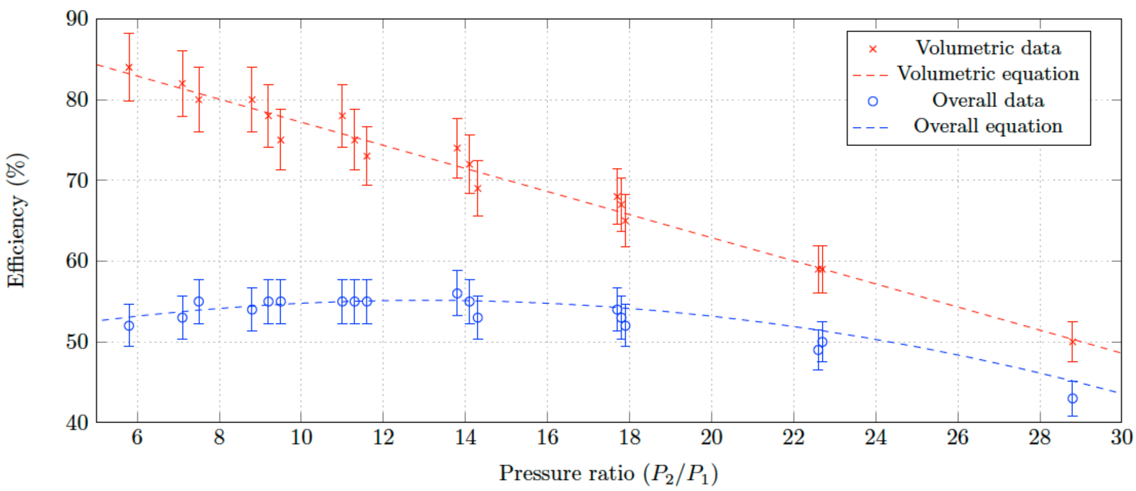

Figure 4: Volumetric and global efficiency of the compressor.

Table 5: Experimental Results

Test	Date	T_a	P_{atm}	T_{dp}	I	u	T_{wi}	T_{wo}	ΔT_{sh}	T_2	T_{sky}	COP
	dd/mm	K	kPa	K	$W.m^{-2}$	$m.s^{-1}$	K	K	K	K	K	
1	12/01	300.25	91.5	290.35	0	0	300.45	317.95	7.1	344.25	300.2±1.0	2.37±0.12
2	13/01	299.75	91.5	293.35	0	0	299.45	318.45	7.1	345.15	299.7±1.0	2.25±0.12
3	16/01	298.05	91.7	298.05	0	0	298.15	319.15	7.1	345.35	298.0±1.0	2.26±0.11
4	17/01	299.25	91.5	290.35	0	0	298.25	319.15	7.1	345.75	299.2±1.0	2.36±0.12
5	19/01	299.65	91.7	291.55	0	0	298.95	318.65	7.1	345.25	299.6±1.0	2.32±0.12
6	23/01	302.85	91.9	288.75	421	0.52	300.75	319.85	7.8	346.35	289.0±1.4	2.56±0.13
7	25/01	306.05	92.0	289.45	709	0.86	301.85	320.55	7.8	347.85	292.4 ±1.4	2.72±0.14
8	25/01	305.85	92.0	289.75	758	0.95	302.45	320.45	7.8	348.55	292.4 ±1.4	2.64±0.14
9	27/01	305.65	92.1	286.65	629	1.16	302.15	319.05	7.8	347.05	290.5 ±1.4	2.69±0.14
10	28/01	304.35	92.1	286.45	811	1.36	302.15	320.95	7.8	346.85	289.2 ±1.4	2.48±0.13

Table 6: Calculate Results

Test	Python		EES	
	COP	T_2	COP	T_2
1	2.29 ±0.04	336.7 ±1.5	2.23 ±0.04	337.6 ±1.5
2	2.31 ±0.04	336.4 ±1.5	2.24 ±0.04	337.2 ±1.4
3	2.30 ±0.04	335.8 ±1.4	2.24 ±0.04	336.5 ±1.4
4	2.30 ±0.04	335.9 ±1.4	2.25 ±0.04	336.7 ±1.4
5	2.31 ±0.04	336.1 ±1.5	2.25 ±0.04	336.9 ±1.4
6	2.55 ±0.05	342.3 ±1.4	2.47 ±0.05	344.0 ±1.4
7	2.73 ±0.06	347.4 ±1.5	2.62 ±0.05	350.0 ±1.5
8	2.75 ±0.06	348.3 ±1.6	2.63 ±0.05	351.0 ±1.5
9	2.70 ±0.06	345.7 ±1.4	2.60 ±0.05	348.1 ±1.5
10	2.76 ±0.06	348.7 ±1.6	2.64 ±0.05	351.4 ±1.5

and calculated COP for the simulation made in Python. The MD and MAD of compressor outlet temperature of the simulation made in EES are respectively 0.97±0.16% and 1.54±0.16%. The MD and MAD of compressor outlet temperature of the simulation made in Python are respectively -1.42±0.16% and 1.53±0.16%.

Only one point for COP using each programming platform (EES and Python) in Figure **5** is outside of the range of ±5%. This point represents the experimental test number 10. Comparing the experimental results in test number 10, the solar radiation, ambient temperature, and wind speed were higher than test 6 and the difference of outlet and inlet water temperature were lower than test number 6, so the COP found experimentally in test number 10 should be bigger than the COP of test 6. This large difference of experimental and theoretical COP for this point is probably due to a failure in the equipment or the measures during the experimental tests. Removing this point the maximum deviation are 3.8%±1.8%, that is lower than the maximum deviation of the models presented by Chyng *et al*. [14], Moreno-Rodríguez *et al*. [45], Mohamed *et al*. [50], Duarte [51], Kong *et al*. [53] and Ma *et al*. [56].

For the COP, the uncertainty of the model was approximately three times lower than obtained experimentally. For the discharge temperature, the uncertainty of the model was 50% higher than that obtained experimentally. The higher uncertainty of the discharge temperature calculated by the model than the discharge temperature was also found in the study present by Duarte *et al*. [104].

With regard to the model uncertainties, for calculating the discharge temperature at outdoor conditions, the input variables that most contribute to this uncertainty are subcooling, superheating and solar radiation, contributing with the following percentages

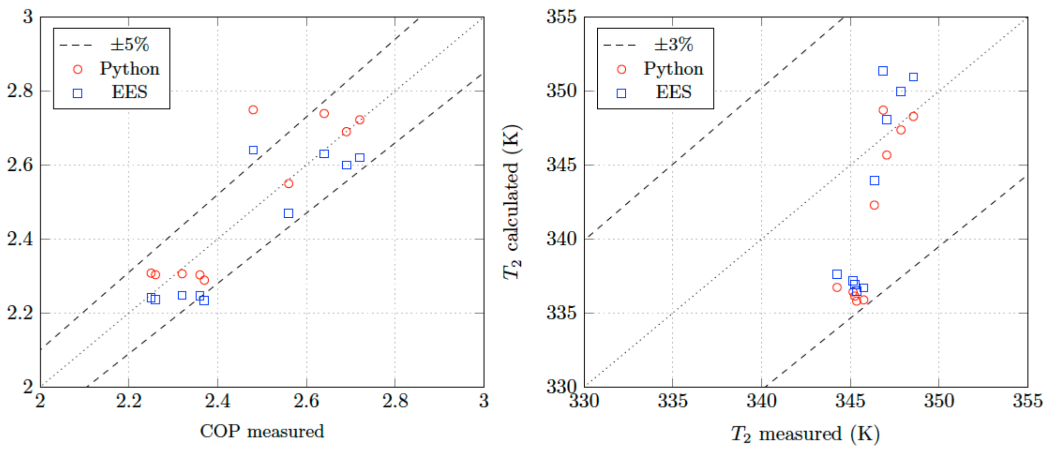

Figure 5: Comparison of theoretical and experimental results using the model in Python and in EES.

46.0%, 20.7% and 15.3%. For COP the uncertainty of subcooling contributes with 28.9% in the uncertainty of superheating with 27.8% the uncertainty of water temperature at the exit of the condenser with 15.6%. For calculating the discharge temperature at indoor conditions, the input variables that most contribute to this uncertainty are subcooling, superheating and temperature of water at inlet of condenser, contributing with the following percentages 47.2%, 29.2% and 15.6%. For COP the uncertainty of subcooling contributes with 17.33% in the uncertainty of superheating with 29.3% the uncertainty of water temperature at the inlet of the condenser with 29.9%.

3.3. Correlation Testing

Some simulations were made testing different correlations to assess their influence on the results. The modifications in the mathematical model were made in the solar collector/evaporator, where the flow conditions can be different from the conditions used for the development of the correlation. For calculating the convective heat transfer coefficient in the refrigerant, four hypotheses were tested. The correlations of Shah [87] (Eq. 19 to 22), Sun and Mishima [90] and Liu and Winterton [89] was used to calculate the convective and the correlation of Gnielinski [92] (Eq. 35) for single-phase flow. The detail description of correlations of Sun and Mishima [90] and Liu and Winterton [89] can be found in Bell and Rutman [97]. The last hypothesis is the same adopted by Deng and Yu [48] that assumed the thermal resistance for convection in the refrigerant side negligible. For calculating the convective heat transfer coefficient in the air five hypotheses were tested. Beyond the equations suggest by Neils and Klein [82] described in the Eq. 12 to 18, the empirical correlations developed in solar collectors and presented by Kumar and Mullick [105], Sharples and Charlesworth [106], Watmuff *et al.* [107] and McAdams [108] were used. These correlations are linear equations as a function of wind speed (u) and are presented in Table **7**.

The mean deviations result for COP and discharge temperature using different correlations are shown in Table **7** and **8**, with their respective uncertainties. For the combination of the hypotheses of Deng and Yu [48] and Kumar and Mullick [105] the mathematical model did not converge. Changes in the correlations for the

Table 7: Mean Deviation of COP using Different Correlation

		Cor. [87]	Cor. [48]	Cor. [90]	Cor. [89]
Neils and Klein [82] (Eq. 12 to 18)	MD MAD	1.2 ±1.8 % 2.6 ±1.8 %	1.6 ±1.8 % 2.7 ±1.8 %	0.9 ±1.8 % 2.6 ±1.8 %	1.3 ±1.8 % 2.6 ±1.8 %
Kumar and Mullick [105] $h = 6.9 + 3.87u$	MD MAD	3.9 ±1.8 % 3.9 ±1.8 %	- -	3.5 ±1.8 % 3.6 ±1.8 %	3.9 ±1.8 % 4.0 ±1.8 %
Sharples and Charlesworth [106] $h = 8.3 + 2.2u$	MD MAD	4.4 ±1.8 % 4.4 ±1.8 %	4.9 ±1.8 % 4.9 ±1.8 %	4.0 ±1.8 % 4.0 ±1.8 %	4.4 ±1.8 % 4.4 ±1.8 %
Watmuff *et al.* [107] $h = 2.8 + 3u$	MD MAD	1.3 ±1.8 % 3.0 ±1.8 %	1.7 ±1.8 % 3.2 ±1.8 %	1.0 ±1.8 % 3.0 ±1.8 %	1.4 ± 1.8 % 3.1 ±1.8 %
McAdams [108] $h = 5.7 + 3.8u$	MD MAD	3.2 ±1.8 % 3.5 ±1.8 %	3.7 ±1.8 % 3.9 ±1.8 %	2.8 ±1.8 % 3.4 ±1.8 %	3.3 ± 1.8 % 3.6 ±1.8 %

Table 8: Mean Deviation of Discharge Temperature using Different Correlation

		Cor. [87]	Cor. [48]	Cor. [90]	Cor. [89]
Neils and Klein [82] (Eq. 12 to 18)	MD MAD	-1.42±0.16 % 1.53±0.16 %	-1.38±0.16 % 1.50±0.16 %	-1.45±0.16 % 1.56±0.16 %	-1.42±0.16 % 1.53±0.16 %
Kumar and Mullick [105] $h = 6.9 + 3.87u$	MD MAD	-1.12±0.16 % 1.37±0.16 %	- -	-1.17±0.16 % 1.39±0.16 %	-1.11±0.16 % 1.37±0.16 %
Sharples and Charlesworth [106] $h = 8.3 + 2.2u$	MD MAD	-1.08±0.16 % 1.32±0.16 %	-1.01±0.16 % 1.32±0.16 %	-1.12±0.16 % 1.34±0.16 %	-1.07±0.16 % 1.32±0.16 %
Watmuff *et al.* [107] $h = 2.8 + 3u$	MD MAD	-1.37±0.16 % 1.52±0.16 %	-1.33±0.16 % 1.52±0.16 %	-1.41±0.16 % 1.54±0.16 %	-1.37±0.16 % 1.52±0.16 %
McAdams [108] $h = 5.7 + 3.8u$	MD MAD	-1.19±0.16 % 1.41±0.16 %	-1.13±0.16 % 1.41±0.16 %	-1.23±0.16 % 1.43±0.16 %	-1.18±0.16 % 1.41±0.16 %

refrigerant did not affect the results if the range of uncertainty is considered, but the correlation for the airside affects strongly the results in both cases. None of the 20 combinations of correlations affected the uncertainty of the MAD and MD. Considering the absolute values, the use of correlation of Sun and Mishima [90] instead of Shah [87] reduces in 0.3% the MD for COP increases only 0.03% the MD for discharge temperature. Additionally, the correlation of Sun and Mishima [90] calculate the average boiling heat transfer coeficient during and Shah [87] local boiling heat transfer coefficient, therefore a numerical integration is required. Finally, the use of correlation of Sun and Mishima [90] instead of Shah [87] reduces the computational time to run in all the simulations listed in Table **5** in 10%. For minimizing the mean difference of discharge temperature another pair of correlations should be chosen.

3.4. Parallel Computing

The CPU utilization on the computer during the first sixty seconds of simulations is shown in Figure **6** considering the simulations in the EES, Python and Python with parallel computing (PPC). Although the Figure **6** does not show the CPU usage during the entire simulation in the remaining time of the simulation the pattern of CPU utilization remained the same as shown in Figure **6**. Simulations using EES and Python without parallel computing are not able to take advantage of all available computer resources and it is possible to see that during almost the entire simulation the CPU usage is around 8-12%, which approximately represents the resource of one core of the CPU. On the other hand, simulations with python and parallel processing use most of the time and all resources available on the computer. There are some valleys in Figure **6** where the CPU utilization drops to approximately 30% which represents the moment which the parallel processing has ended and a CPU is gathering the results of that simulation and preparing new simulations for the parallel processing. The total simulation times to perform the calculations involving a set of correlations is shown in Figure **7** using the different strategies and software mentioned above. Using python with parallel processing reduced the simulation time by 88% compared to the EES simulation time.

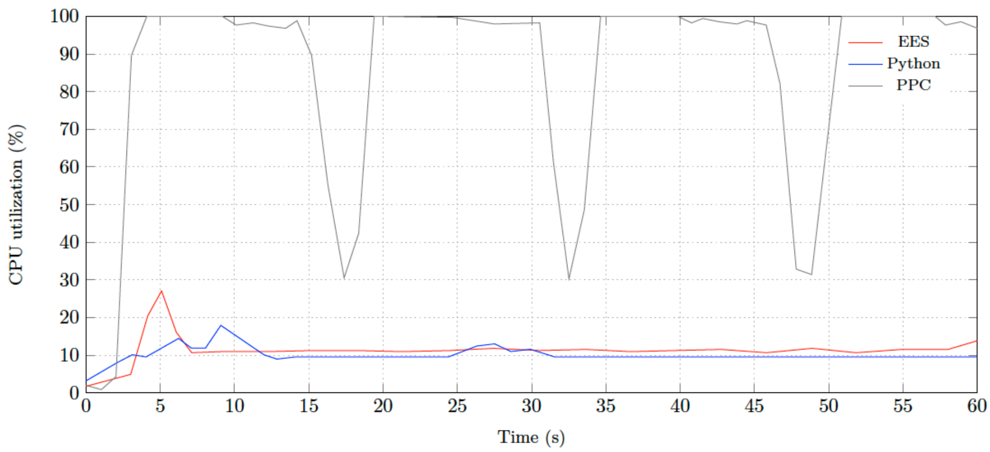

Figure 6: CPU utilization during the first sixty seconds of the simulation.

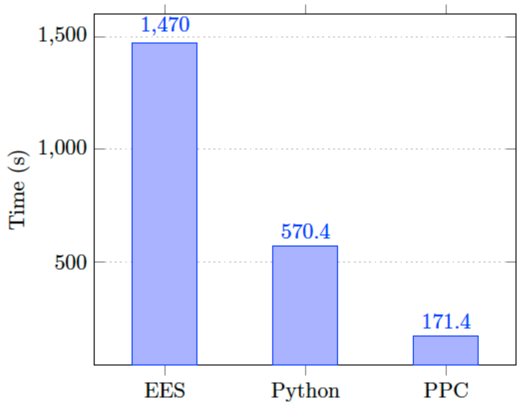

Figure 7: Total time of simulation.

The Python code that can be found in the link at the end of the paper not only presents the mathematical model of the heat pump, but also a series of functions that can be used in different models and problems involving thermodynamic, heat transfer and fluid. Finally, a generalized function to calculate uncertainty using parallel processing any mathematical model in Python is also presented. The function for calculating uncertainty using parallel processing was validated comparing the uncertainty results with the native functionality of EES for calculating uncertainty. This comparison was not only made with the mathematical model presented in this study, but with other simple

Nomenclature					
Greek Symbols		L	Length $[m]$	3	expansion valve inlet or condenser outlet
β	coefficient of thermal expansion $[K^{-1}]$	E	error [%]	4	expansion valve outlet or evaporator inlet
δ	fin thickness [m]	MAD	mean absolute deviation	a	air
ϵ	rugosity $[m]$	MD	mean absolute deviation	$calc$	calculated
η	efficiency	n	rotation speed $[s^{-1}]$	ch	characteristic
μ	viscosity $[Pa.s]$	NTU	number of transfer units	col	collector
ρ	mass density $[kg.m^{-3}]$	P	pressure $[Pa]$	$cond$	condenser
σ	Stefane-Boltzmann constant $[W.m^{-2}K^{-4}]$	p	reduced pressure	$crit$	critical
σ'	surface tension $[N.m^{-1}]$	q	heat flux $[W.m^{-2}]$	dp	dew point
θ	inclination of collector $[rad]$	S	net radiation absolved per unit of area $[W.m^{-2}]$	ev	evaporator
ε	emissivity	T	temperature $[K]$	exp	experimental
ξ	effectiveness	t	temperature uncertainty $[K]$	g	global efficiency
ξ'	effectiveness	U	overall heat transfer coefficient $[W.m^{-2}K^{-1}]$	I	flow regime I during condensation
ζ	heat leakage coefficient	u	wind velocity $[m.s^{-1}]$	i	inner
Latin Symbols		V	volume $[m^3]$	II	flow regime II during condensation
$\dot{C}$	heat capacity rate $[W.K^{-1}]$	v	vapor velocity [dimensionless]	ii	inner tube inside geometry
$\dot{m}$	mass flow rate $[kg.s^{-1}]$	W	distance between the tubes $[m]$	III	flow regime III during condensation
$\dot{Q}$	heat transfer rate $[W]$	x	vapor quality	io	outer tube inside geometry
$\dot{W}$	power $[W]$	**Classical dimensionless numbers**		L	liquid
A	area $[m^2]$	Bo	Boiling	lo	Liquid only
a	absorptivity	Co	Convection	o	outer
B	auxiliary variable	f	Darcy friction factor	oi	inner tube outside geometry
C	heat capacity at constant pressure $[J.kg^{-1}K^{-1}]$	Fr	Froude	oo	outer tube outside geometry
COP	coefficient of performance	Nu	Nusselt	po	pool boiling correlation
D	diameter [m]	Pe	Péclet	r	refrigerant
F	fin efficiency factor	Pr	Prandtl	s	swept volume
F'	collector efficiency factor	Ra	Rayleigh	sky	sky
G	mass velocity $[kg.m^{-2}s^{-1}]$	Re	Reynolds	t	tank
g	gravity $[m.s^{-2}]$	We	Weber	V	vapor
h	convective coefficient $[W.m^{-2}K^{-1}]$	**Subscripts**		vol	volumetric
I	solar radiation intensity $[W.m^{-2}]$	1	compressor inlet or evaporator outlet	w	water
i	specific enthalpy $[J.kg^{-1}]$	2	compressor outlet or condenser inlet	wi	water inlet
k	thermal conductivity $[W.m^{-1}K^{-1}]$	$2s$	compressor outlet considering an isentropic process	wo	water outlet

functions such as the equation for calculating the experimental COP.

4. CONCLUSIONS

A mathematical model of an R134a DX-SAHP for generating residential hot water was utilized in this study to evaluate the performance of simulation findings with practical observations. The theoretical and actual compressor discharge temperature and COP were evaluated using ten experimental experiments performed in various climatic conditions. The following key findings were reached:

- The difference between the results using EES and using Python was small 1.4%. Since in both approaches the same equations were utilized, the difference in the results is probably related to the refrigeration fluid properties library employed in each platform.
- The mean deviation between experimental and theoretical results can be minimized if different correlations are chosen. The use of the correlation proposed by un and Mishima [90] instead of Shah [87] reduced in 0.3% the MD for COP
- The correlations for convective heat transfer coefficient considered in this work had no effect in the uncertainty of the model.
- The correlation for convective heat transfer coefficient for the airside in the evaporator/solar collector had more influence on the results than the correlation for the refrigerant side.
- The use of Python with parallel computing, for uncertainty analyses, reduced the simulation time in 88%.
- The input variables uncertainty that has more impact in the uncertainty of output variables are subcooling and superheating.

5. ACKNOWLEDGEMENTS

This work was supported by Foundation for Research Support of the State of Minas Gerais (FAPEMIG) and National Council for Scientific and Technological Development (CNPq). This study was financed in part by the Coordenação de Aperfeiçoamento de Pessoal de Nível Superior – Brasil (CAPES) – Finance Code 001. Link to Python model:

https://colab.research.google.com/drive/1RpAE8mSTS6zsrCTS16TnYEztjAhgEyxU?usp=sharing

REFERENCES

[1] Kong X, Yang Y, Zhang M, Li Y, Li J. Experimental investigation on a direct-expansion solar-assisted heat pump water heater using r290 with micro-channel heat transfer technology during the winter period. International Journal of Refrigeration 2020; 113: 38-48. https://doi.org/10.1016/j.ijrefrig.2020.01.019

[2] Duarte WM, Rabelo SN, Paulino TF, Pabón JJ, Machado L. Experimental performance analysis of a CO2 directexpansion solar assisted heat pump water heater. International Journal of Refrigeration 2021; 125: 52-63. https://doi.org/10.1016/j.ijrefrig.2021.01.008

[3] Humia GM, Duarte WM, Pabon JJG, de Freitas Paulino T, Machado L. Experimental study and simulation model of a direct expansion solar assisted heat pump to CO2 for water heating: Inventory, coefficient of performance and total equivalent warming impact. Solar Energy 2021; 230: 278-97. https://doi.org/10.1016/j.solener.2021.10.018

[4] Xia L, Ma Z, Kokogiannakis G, Wang Z, Wang S. A model-based design optimization strategy for ground source heat pump systems with integrated photovoltaic thermal collectors. Applied Energy 2018; 214: 178-90. https://doi.org/10.1016/j.apenergy.2018.01.067

[5] Qi D, Pu L, Ma Z, Xia L, Li Y. Effects of ground heat exchangers with different connection configurations on the heating performance of gshp systems. Geothermics 2019; 80: 20-30. https://doi.org/10.1016/j.geothermics.2019.02.002

[6] Ma Z, Xia L, Gong X, Kokogiannakis G, Wang S, Zhou X. Recent advances and development in optimal design and control of ground source heat pump systems. Renewable and Sustainable Energy Reviews 2020; 131: 110001. https://doi.org/10.1016/j.rser.2020.110001

[7] Li H, Campana PE, Tan Y, Yan J. Feasibility study about using a stand-alone wind power driven heat pump for space heating. Applied Energy 2018; 228: 1486 -98. https://doi.org/10.1016/j.apenergy.2018.06.146

[8] Wu J, Ma Y. Experimental study on performance of a biogas engine driven air source heat pump system powered by renewable landfill gas. International Journal of Refrigeration 2016; 62: 19-29. https://doi.org/10.1016/j.ijrefrig.2015.08.023

[9] Buker M, Riffat SB. Solar assisted heat pump systems for low temperature water heating applications: A systematic review. Renewable and Sustainable Energy Reviews 2016; 55: 399 - 413. https://doi.org/10.1016/j.rser.2015.10.157

[10] Faria RN, Nunes RO, Koury RNN, Machado L. Dynamic modeling study for a solar evaporator with expansion valve assembly of a transcritical CO2 heat pump. International Journal of Refrigeration 2016; 64: 203-13. https://doi.org/10.1016/j.ijrefrig.2016.01.004

[11] de Oliveira RN, Faria RN, Antonanzas-Torres F, Machado L, Koury RNN. Dynamic model and experimental validation for a gas cooler of a CO2 heat pump for heating residential water. Science and Technology for the Built Environment 2016; 22(1): 30-40. https://doi.org/10.1080/23744731.2015.1070647

[12] Scarpa F, Tagliafico LA. Exploitation of humid air latent heat by means of solar assisted heat pumps operating below the dew point. Applied Thermal Engineering 2016; 100: 820 -8. https://doi.org/10.1016/j.applthermaleng.2015.12.077

[13] Paulino TF, Oliveira RN, Maia AAT, Palm B, Machado L. Modeling and experimental analysis of the solar radiation in a CO2 direct-expansion solar-assisted heat pump. Applied Thermal Engineering 2019; 148: 160 -72. https://doi.org/10.1016/j.applthermaleng.2018.11.045

[14] Chyng J, Lee C, Huang B. Performance analysis of a solar-assisted heat pump water heater. Solar Energy 2003; 74(1): 33 - 44. https://doi.org/10.1016/S0038-092X(03)00110-5

[15] Torres-Reyes E, Gortari JC. Optimal performance of an irreversible solar-assisted heat pump. Exergy, An

International Journal 2001; 1(2): 107 -11. https://doi.org/10.1016/S1164-0235(01)00016-4

[16] Hawlader M, Chou S, Ullah M. The performance of a solar assisted heat pump water heating system. Applied Thermal Engineering 2001; 21(10): 1049 -65. https://doi.org/10.1016/S1359-4311(00)00105-8

[17] Ito S, Miura N, Wang K. Performance of a heat pump using direct expansion solar collectors. Solar Energy 1999; 65: 189-96. https://doi.org/10.1016/S0038-092X(98)00124-8

[18] Chaturvedi S, Chen D, Kheireddine A. Thermal performance of a variable capacity direct expansion solar-assisted heat pump. Energy Conversion and management 1998; 39(3): 181-91. https://doi.org/10.1016/S0196-8904(96)00228-2

[19] Chaturvedi SK, Shen JY. Thermal performance of a direct expansion solar-assisted heat pump. Solar Energy 1984; 33(2): 155 -62. https://doi.org/10.1016/0038-092X(84)90233-0

[20] ASME. Standard for Verification and Validation in Computational Fluid Dynamics and Heat Transfer: An American National Standard. American Society of Mechanical Engineers; 2009.

[21] BIPM, IEC, IFCC, ILAC, IUPAC, IUPAP, *et al*. Evaluation of measurement data-Guide for the expression of uncertainty in measurement. JCGM 100: 2008. 2008.

[22] Zhang Y, Akkurt N, Yuan J, Xiao Z, Wang Q, Gang W. Study on model uncertainty of water source heat pump and impact on decision making. Energy and Buildings 2020; 216: 109950. https://doi.org/10.1016/j.enbuild.2020.109950

[23] Zhang Y, Cui C, Yuan J, Zhang C, Gang W. Quantification of model uncertainty of water source heat pump and impacts on energy performance. In: IOP Conference Series: Earth and Environmental Science; vol. 238. IOP Publishing; 2019, p. 012067. https://doi.org/10.1088/1755-1315/238/1/012067

[24] Frutiger J, Zühlsdorf B, Elmegaard B, Abildskov J, Sin G. Reverse engineering of working fluid selection for industrial heat pump based on monte carlo sampling and uncertainty analysis. Industrial & Engineering Chemistry Research 2018; 57(40): 13463-77. https://doi.org/10.1021/acs.iecr.7b04607

[25] Coppitters D, De Paepe W, Contino F. Robust design optimization of a photovoltaic-battery-heat pump system with thermal storage under aleatory and epistemic uncertainty. Energy 2021; 229: 120692. https://doi.org/10.1016/j.energy.2021.120692

[26] Moarry DP. Modeling and operation of ground source heat pumps in electricity markets considering uncertainty. Ph.D. thesis; University of Waterloo; 2022.

[27] Nielsen MG, Morales JM, Zugno M, Pedersen TE, Madsen H. Economic valuation of heat pumps and electric boilers in the danish energy system. Applied Energy 2016; 167: 189-200. https://doi.org/10.1016/j.apenergy.2015.08.115

[28] Chow TT, Bai Y, Fong K, Lin Z. Analysis of a solar assisted heat pump system for indoor swimming pool water and space heating. Applied energy 2012; 100: 309-17. https://doi.org/10.1016/j.apenergy.2012.05.058

[29] Panaras G, Mathioulakis E, Belessiotis” V. Investigation of the performance of a combined solar thermal heat pump hot water system. Solar Energy 2013; 93: 169 -82. https://doi.org/10.1016/j.solener.2013.03.027

[30] Magraner T, Montero A, Quilis S, Urchueguía J. Comparison between design and actual energy performance of a hvac-ground coupled heat pump system in cooling and heating operation. Energy and buildings 2010; 42(9): 1394-401. https://doi.org/10.1016/j.enbuild.2010.03.008

[31] Fan R, Gao Y, Hua L, Deng X, Shi J. Thermal performance and operation strategy optimization for a practical hybrid ground-source heat-pump system. Energy and Buildings 2014; 78: 238-47. https://doi.org/10.1016/j.enbuild.2014.04.041

[32] Pu L, Qi D, Xu L, Li Y. Optimization on the performance of ground heat exchangers for gshp using kriging model based on moga. Applied Thermal Engineering 2017; 118: 480-9. https://doi.org/10.1016/j.applthermaleng.2017.02.114

[33] Pärisch P, Mercker O, Warmuth J, Tepe R, Bertram E, Rockendorf G. Investigations and model validation of a ground-coupled heat pump for the combination with solar collectors. Applied Thermal Engineering 2014; 62(2): 375-81. https://doi.org/10.1016/j.applthermaleng.2013.09.016

[34] Koury R, Machado L, Ismail K. Numerical simulation of a variable speed refrigeration system. International journal of refrigeration 2001; 24(2): 192-200. https://doi.org/10.1016/S0140-7007(00)00014-1

[35] Daviran S, Kasaeian A, Golzari S, Mahian O, Nasirivatan S, Wongwises S. A comparative study on the performance of hfo-1234yf and hfc-134a as an alternative in automotive air conditioning systems. Applied Thermal Engineering 2017; 110: 1091-100. https://doi.org/10.1016/j.applthermaleng.2016.09.034

[36] D'Agaro P, Coppola M, Cortella G. Field tests, model validation and performance of a co2 commercial refrigeration plant integrated with hvac system. International Journal of Refrigeration 2019; 100: 380-91. https://doi.org/10.1016/j.ijrefrig.2019.01.030

[37] Tsui C, Yan AY, Lai H. Speeding up monte carlo computations by parallel processing using a gpu for uncertainty evaluation in accordance with gum supplement 2. NCSLI Measure 2018; 12(3): 41-56. https://doi.org/10.1080/19315775.2019.1710003

[38] Gao Y, Hang Y, Yang M. A cooling load prediction method using improved ceemdan and markov chains correction. Journal of Building Engineering 2021; 42: 103041. https://doi.org/10.1016/j.jobe.2021.103041

[39] Tavakolan M, Mostafazadeh F, Eirdmousa SJ, Safari A, Mirzaei K. A parallel computing simulation-based multiobjective optimization framework for economic analysis of building energy retrofit: A case study in iran. Journal of Building Engineering 2022; 45: 103485. https://doi.org/10.1016/j.jobe.2021.103485

[40] Kuang Y, Sumathy K, Wang R. Study on a direct-expansion solar-assisted heat pump water heating system. International Journal of Energy Research 2003; 27(5): 531-48. https://doi.org/10.1002/er.893

[41] Chata FG, Chaturvedi S, Almogbel A. Analysis of a direct expansion solar assisted heat pump using different refrigerants. Energy Conversion and Management 2005; 46(15): 2614-24. https://doi.org/10.1016/j.enconman.2004.12.001

[42] Xu G, Deng S, Zhang X, Yang L, Zhang Y. Simulation of a photovoltaic/thermal heat pump system having a modified collector/evaporator. Solar Energy 2009; 83(11): 1967 -76. https://doi.org/10.1016/j.solener.2009.07.008

[43] Chow TT, Pei G, Fong K, Lin Z, Chan A, He M. Modeling and application of direct-expansion solar-assisted heat pump for water heating in subtropical hong kong. Applied Energy 2010; 87(2): 643-9. https://doi.org/10.1016/j.apenergy.2009.05.036

[44] Kong X, Zhang D, Li Y, Yang Q. Thermal performance analysis of a direct-expansion solar-assisted heat pump water heater. Energy 2011; 36(12): 6830-8. https://doi.org/10.1016/j.energy.2011.10.013

[45] Moreno-Rodríguez A, González-Gil A, Izquierdo M, Garcia-Hernando N. Theoretical model and experimental validation of a direct-expansion solar assisted heat pump for domestic hot water applications. Energy 2012; 45(1): 704-15. https://doi.org/10.1016/j.energy.2012.07.021

[46] Chaturvedi S, Gagrani V, Abdel-Salam T. Solar-assisted heat pump - a sustainable system for low-temperature water heating applications. Energy Conversion and Management 2014; 77: 550-7. https://doi.org/10.1016/j.enconman.2013.09.050

[47] Sun X, Dai Y, Novakovic V, Wu J, Wang R. Performance comparison of direct expansion solar-assisted heat pump

and conventional air source heat pump for domestic hot water. Energy Procedia 2015; 70: 394 - 401. https://doi.org/10.1016/j.egypro.2015.02.140

[48] Deng W, Yu J. Simulation analysis on dynamic performance of a combined solar/air dual source heat pump water heater. Energy Conversion and Management 2016; 120: 378 -87. https://doi.org/10.1016/j.enconman.2016.04.102

[49] Kong X, Li Y, Lin L, Yang Y. Modeling evaluation of a direct-expansion solar-assisted heat pump water heater using R410A. International Journal of Refrigeration 2017; 76: 136-46. https://doi.org/10.1016/j.ijrefrig.2017.01.020

[50] Mohamed E, Riffat S, Omer S. Low-temperature solar-plate-assisted heat pump: A developed design for domestic applications in cold climate. International Journal of Refrigeration 2017; 81: 134 -50. https://doi.org/10.1016/j.ijrefrig.2017.05.020

[51] Duarte WM. Numeric model of a direct expansion solar assisted heat pump water heater operating with low GWP refrigerants (R1234yf, R290, R600a and R744) for replacement of R134a. Ph.D. thesis; UFMG; 2018.

[52] Rabelo SN, Paulino TF, Machado L, Duarte WM. Economic analysis and design optimization of a direct expansion solar assisted heat pump. Solar Energy 2019; 188: 164 -74. https://doi.org/10.1016/j.solener.2019.05.072

[53] Kong X, Wang B, Shang Y, Li J, Li Y. Influence of different regulation modes of compressor speed on the performance of direct-expansion solar-assisted heat pump water heater. Applied Thermal Engineering 2020; 169: 115007. https://doi.org/10.1016/j.applthermaleng.2020.115007

[54] Diniz HAG, Paulino TF, Pabon JJG, Maia AAT, Oliveira RN. Dynamic model of a transcritical co2 heat pump for residential water heating. Sustainability 2021; 13(6). https://doi.org/10.3390/su13063464

[55] Wang B, Kong X, Yan X, Shang Y, Li Y. Influence of subcooling on performance of direct-expansion solar-assisted heat pump. International Journal of Refrigeration 2021; 122: 201-9. https://doi.org/10.1016/j.ijrefrig.2020.10.037

[56] Ma K, Wang Z, Li X, Wu P, Li S. Structural optimization of collector/evaporator of direct-expansion solar/airassisted heat pump. Alexandria Engineering Journal 2021; 60(1): 387-92. https://doi.org/10.1016/j.aej.2020.08.039

[57] Dai R, Tian R, Zheng S, Wei M, Shi G. Dynamic performance evaluation of lng vaporization system integrated with solar-assisted heat pump. Renewable Energy 2022; 188: 561-72. https://doi.org/10.1016/j.renene.2022.02.062

[58] Humia GM. Estudo experimental e modelo de simulação do inventário de refrigerante em uma bomba de calor a CO2 dotada de evaporador solar. Ph.D. thesis; UFMG; 2022.

[59] Kara O, Ulgen K, Hepbasli A. Exergetic assessment of direct-expansion solar-assisted heat pump systems: review and modeling. Renewable and Sustainable Energy Reviews 2008; 12(5): 1383-401. https://doi.org/10.1016/j.rser.2006.12.001

[60] Omojaro P, Breitkopf C. Direct expansion solar assisted heat pumps: A review of applications and recent research. Renewable and Sustainable Energy Reviews 2013; 22: 33 - 45. https://doi.org/10.1016/j.rser.2013.01.029

[61] Mohanraj M, Belyayev Y, Jayaraj S, Kaltayev A. Research and developments on solar assisted compression heat pump systems - A comprehensive review (Part A: Modeling and modifications). Renewable and Sustainable Energy Reviews 2018; 83: 90 - 123. https://doi.org/10.1016/j.rser.2017.08.022

[62] Mohanraj M, Belyayev Y, Jayaraj S, Kaltayev A. Research and developments on solar assisted compression heat pump systems - A comprehensive review (Part-B: Applications). Renewable and Sustainable Energy Reviews 2018; 83: 124 -55. https://doi.org/10.1016/j.rser.2017.08.086

[63] de Paula CH, Duarte WM, Rocha TTM, de Oliveira RN, Maia AAT. Energetic, exergetic, environmental, and economic assessment of a cascade refrigeration system operating with four different ecological refrigerant pairs. International Journal of Air-Conditioning and Refrigeration 2021; 29(03): 2150025. https://doi.org/10.1142/S2010132521500255

[64] Duprez ME, Dumont E, Frère M. Modelling of reciprocating and scroll compressors. International Journal of Refrigeration 2007; 30(5): 873-86. https://doi.org/10.1016/j.ijrefrig.2006.11.014

[65] Ndiaye D, Bernier M. Dynamic model of a hermetic reciprocating compressor in on-off cycling operation (abbreviation: Compressor dynamic model). Applied Thermal Engineering 2010; 30(8): 792-9. https://doi.org/10.1016/j.applthermaleng.2009.12.007

[66] Bell IH, Ziviani D, Lemort V, Bradshaw CR, Mathison M, Horton WT, *et al*. Pdsim: A general quasi-steady modeling approach for positive displacement compressors and expanders. International Journal of Refrigeration 2020; 110: 310-22. https://doi.org/10.1016/j.ijrefrig.2019.09.002

[67] de Paula CH, Duarte WM, Rocha TTM, de Oliveira RN, Maia AAT. Optimal design and environmental, energy and exergy analysis of a vapor compression refrigeration system using r290, r1234yf, and r744 as alternatives to replace r134a. International Journal of Refrigeration 2020; 113: 10-20. https://doi.org/10.1016/j.ijrefrig.2020.01.012

[68] Xu Y, Mao C, Zhang X, Shen X, Huang Y, Chen G. Optimization on integrated inverter-compressor co2 heat pump with new operating model. Applied Thermal Engineering 2022; 200: 117632. https://doi.org/10.1016/j.applthermaleng.2021.117632

[69] F-Chart Software. Equation engineering solver v10.643. 2019.

[70] Bell IH, Wronski J, Quoilin S, Lemort V. Pure and pseudo-pure fluid thermophysical property evaluation and the open-source thermophysical property library coolprop. Industrial & Engineering Chemistry Research 2014; 53(6): 2498-508. https://doi.org/10.1021/ie4033999

[71] Minetto S. Theoretical and experimental analysis of a CO2 heat pump for domestic hot water. International journal of refrigeration 2011; 34(3): 742-51. https://doi.org/10.1016/j.ijrefrig.2010.12.018

[72] Duarte WM, Paulino TF, Tavares SG, Cançado KN, Machado L. Comparative study of geothermal and conventional air conditioner: A case of study for office applications. Journal of Building Engineering 2023; 105786. https://doi.org/10.1016/j.jobe.2022.105786

[73] Laughman CR, Qiao H, Aute V, Radermacher R. A comparison of transient heat pump cycle models using alternative flow descriptions. Science and Technology for the Built Environment 2015; 21(5): 666-80. https://doi.org/10.1080/23744731.2015.1040342

[74] Nunes R, Castro L, Machado L, Koury R. Distributed and nonsteady-state model of an air cooler working with R22 and R410A. International Journal of Air-Conditioning and Refrigeration 2016; 24(02): 1650008. https://doi.org/10.1142/S2010132516500085

[75] Garcia J, Ali T, Duarte WM, Khosravi A, Machado L. Comparison of transient response of an evaporator model for water refrigeration system working with r1234yf as a drop-in replacement for r134a. International Journal of Refrigeration 2018; 91: 211-22. https://doi.org/10.1016/j.ijrefrig.2018.04.026

[76] Li W, Chu Y, Xu P, Yang Z, Ji Y, Ni L, *et al*. A transient model for the thermal inertia of chilled-water systems during demand response. Energy and Buildings 2017; 150: 383-95. https://doi.org/10.1016/j.enbuild.2017.05.078

[77] de Paula CH, Duarte WM, Rocha TTM, de Oliveira RN, de Paoli Mendes R, Maia AAT. Thermo-economic and environmental analysis of a small capacity vapor compression refrigeration system using R290, R1234yf, and R600a. International Journal of Refrigeration 2020; 118:

250-60.
https://doi.org/10.1016/j.ijrefrig.2020.07.003

[78] Duarte WM, Paulino TF, Tavares SG, Maia AA, Machado L. Feasibility of solar-geothermal hybrid source heat pump for producing domestic hot water in hot climates. International Journal of Refrigeration 2021; 124: 184-96. https://doi.org/10.1016/j.ijrefrig.2020.12.022

[79] Gliah O, Kruczek B, Etemad SG, Thibault J. The effective sky temperature: an enigmatic concept. Heat and mass transfer 2011; 47(9): 1171-80. https://doi.org/10.1007/s00231-011-0780-1

[80] Berdahl P, Fromberg R. The thermal radiance of clear skies. Solar Energy 1982; 29(4): 299-314. https://doi.org/10.1016/0038-092X(82)90245-6

[81] Bergman TL, Lavine AS, Incropera FP, DeWitt DP. Introduction to heat transfer. John Wiley & Sons; 2011.

[82] Neils G, Klein S. Heat Transfer. Cambridge university press; 2009.

[83] ASHRAE. ASHRAE Handbook - Fundamentals (SI Edition). American Society of Heating, Refrigerating and Air-Conditioning Engineers, Inc.; 2013. ISBN 978-1-936504-46-6.

[84] Lloyd J, Moran W. Natural convection adjacent to horizontal surface of various planforms. Journal of Heat Transfer 1974; 96(4): 443-7. https://doi.org/10.1115/1.3450224

[85] Churchill SW, Chu HHS. Correlating equations for laminar and turbulent free convection from a vertical plate. International Journal of Heat and Mass Transfer 1975; 18(11): 1323 -9. https://doi.org/10.1016/0017-9310(75)90243-4

[86] Churchill SW, Ozoe H. Correlations for laminar forced convection in flow over an isothermal flat plate and in developing and fully developed flow in an isothermal tube. Journal of Heat Transfer 1973. https://doi.org/10.1115/1.3450078

[87] Shah MM. Unified correlation for heat transfer during boiling in plain mini/micro and conventional channels. International Journal of Refrigeration 2017; 74: 604-24. https://doi.org/10.1016/j.ijrefrig.2016.11.023

[88] Dittus FW, Boelter M. Heat transfer in automobile radiators of the tubler type. Univ Calif Pubs Eng 1930; 2: 443.

[89] Liu Z, Winterton R. A general correlation for saturated and subcooled flow boiling in tubes and annuli, based on a nucleate pool boiling equation. International journal of heat and mass transfer 1991; 34(11): 2759-66. https://doi.org/10.1016/0017-9310(91)90234-6

[90] Sun L, Mishima K. An evaluation of prediction methods for saturated flow boiling heat transfer in mini-channels. International Journal of Heat and Mass Transfer 2009; 52(23-24): 5323-9. https://doi.org/10.1016/j.ijheatmasstransfer.2009.06.041

[91] Cooper M. Saturated nucleate pool boiling-a simple correlation. In: 1st UK National Heat Transfer Conference, 1984. 1984, p. 785-93. https://doi.org/10.1016/B978-0-85295-175-0.50013-8

[92] Gnielinski V. New equations for heat and mass transfer in turbulent pipe and channel flow. Int Chem Eng 1976; 16(2): 359-68.

[93] Rohsenow WM, Hartnett JP, Cho YI, *et al*. Handbook of heat transfer; vol. 3. McGraw-Hill, New York; 1998.

[94] Zigrang D, Sylvester N. Explicit approximations to the solution of colebrook's friction factor equation. AIChE Journal 1982; 28(3): 514-5. https://doi.org/10.1002/aic.690280323

[95] Shah MM. Comprehensive correlations for heat transfer during condensation in conventional and mini/micro channels in all orientations. International journal of refrigeration 2016; 67: 22-41. https://doi.org/10.1016/j.ijrefrig.2016.03.014

[96] Chapra SC, Canale RP, *et al*. Numerical methods for engineers. Boston: McGraw-Hill Higher Education,; 2010.

[97] Bell C, Rutman J. Calebbell/ht: Heat transfer component of chemical engineering design library (ChEDL). 2021

[98] Bell C, Volpatto D, Killam R, Kremitzki K, B A, KEVIN G, *et al*. Calebbell/fluids: 1.0.0 release. 2021.

[99] BIPM, IEC, IFCC, ILAC, IUPAC, IUPAP, *et al*. Evaluation of measurement data-supplement 1 to the'guide to the expression of uncertainty in measurement: Propagation of distributions using a monte carlo method. Bureau international des poids et mesures - BIPM 2008.

[100] Jalid A, Hariri S, El Gharad A, Senelaer JP. Comparison of the gum and monte carlo methods on the flatness uncertainty estimation in coordinate measuring machine. International Journal of Metrology and Quality Engineering 2016; 7(3): 302. https://doi.org/10.1051/ijmqe/2016013

[101] Mahmoud GM, Hegazy RS. Comparison of gum and monte carlo methods for the uncertainty estimation in hardness measurements. International Journal of Metrology and Quality Engineering 2017; 8: 14. https://doi.org/10.1051/ijmqe/2017014

[102] Soares DSL. Sobre o valor da aceleração da gravidade medido no departamento de física. 2011. URL: http: //goo.gl/ilqYmq.

[103] Diniz HAG. Estudo comparativo da eficiência energética de uma bomba de calor assistida por energia solar operando com condensadores por imersão e coaxial. Master's thesis; UFMG; Belo Horizonte, MG, Brazil; 2017.

[104] Duarte WM, Pabon JJG, Maia AAT, Machado L. Nonisentropic phenomenological model of a reciprocating compressor. International Journal of Air-Conditioning and Refrigeration 2019: 1950039. https://doi.org/10.1142/S2010132519500391

[105] Kumar S, Mullick S. Wind heat transfer coefficient in solar collectors in outdoor conditions. Solar Energy 2010; 84(6): 956-63. https://doi.org/10.1016/j.solener.2010.03.003

[106] Sharples S, Charlesworth P. Full-scale measurements of wind-induced convective heat transfer from a roof-mounted flat plate solar collector. Solar Energy 1998; 62(2): 69-77. https://doi.org/10.1016/S0038-092X(97)00119-9

[107] Watmuff J, Charters W, Proctor D. Solar and wind induced external coefficients for solar collectors. comples, 2. Rev Inter Heliotech, Marseille 1977.

[108] McAdams WH. Heat transmission. Tech. Rep.; 1954.

Received on 01-04-2023 Accepted on 04-05-2023 Published on 16-05-2023

DOI: https://doi.org/10.31875/2410-2199.2023.10.02